G. Gori, M. Zocca, M. Garabelli, A. Guardone, G. Quaranta
PoliMIce: a Simulation Framework for Three-Dimensional Ice Accretion
Applied Mathematics and Computation, Vol. 267, 2015, p. 96-107
doi:10.1016/j.amc.2015.05.081

PoliMIce: An Simulation Framework for Three-dimensional Ice Accretion

G. Gori, M. Zocca, M. Garabelli, A. Guardone [*], G. Quaranta

Department of Aerospace Science and Technology, Politecnico di Milano via La Masa, 34, 20156 Milano, Italy

Abstract

A modeling framework is developed to perform two- and three-dimensional simulations of ice accretion over solid bodies in a wet air flow. The PoliMIce (Politecnico di Milano Ice accretion software) library provides a general interface allowing different aerodynamic and ice accretion software to communicate. The built-in ice accretion engine moves from the well-known Myers approach and it includes state-of-the-art ice formation models. The ice accretion engine implements a fully three-dimensional representation of the two-phase flow over the solid body, accounting for both rime and glaze ice formation. As an improvement over the reference model, a parabolic temperature profile is assumed to guarantee the consistency with respect to the wall boundary conditions. Moreover, the mass balance is generalized to conserve the liquid fraction at the interface between the glaze and the rime ice types. Numerical simulations are presented regarding in-flight ice accretion over two-dimensional airfoils and three-dimensional straight- and swept-wings. The CFD open-source software OpenFOAM was used to compute the aerodynamic field and the droplet trajectories. Simulation results compare fairly well with available experiments on ice accretion.

Key words: ice accretion; CFD; Stefan problem; two-phase flows

1 Introduction

A wide number of catastrophic crashes in aviation is directly or indirectly related to the occurrence of ice formation. The icing phenomenon affects aircraft flying in severe conditions, like those that can be encountered in clouds

[*] Corresponding author
Email address: `alberto.guardone@polimi.it` (G. Quaranta).

composed by super-cooled droplets, namely, droplets in a state of unstable thermo-mechanical equilibrium that is possibly perturbed upon impact on the surface, generating water freezing [8].

Ice formations are classified as either *rime* or *glaze* ice. The former typically occurs at very low temperature: when super-cooled droplets hit the surface of the plane, their unstable equilibrium is perturbed and water instantaneously freezes. This causes small air bubbles to remain trapped within the ice, so the resulting ice is characterized by an opaque aspect. If instead the temperature is closer to the melting point, droplets first impact the surface and flows over it before freezing: the circumstance permits air bubbles to separate from water and hence the resulting ice has an homogeneous structure characterized by a typical transparent look, producing what we usually call glaze ice. This type of ice is always covered by a thin liquid film, giving it a lucid aspect. The density of glaze ice is usually higher than that of rime ice [13, 15, 18].

Ice formation over an aircraft causes a significant increase in weight. It can possibly choke the air manifold of the engine and it may result in the locking of inner mechanisms such as aerodynamic control surfaces or high-lift devices. Moreover, the occurrence of ice can affect aircraft instrumentation in general and measurement instruments in particular, thus presenting misleading information to the pilot. The most prominent effect of ice formation is possibly the change in the airfoil shape, which implies a dramatic degradation of aerodynamic performances: a reduction of lift and an increase of drag. The formation of ice over the blades of the first stage of a turbofan compressor can lead to an engine failure due to the ice shedding which causes direct impact damages and indirect damages due to structural unbalancing.

The interest towards ice accretion is not limited to aeronautical applications: a considerable amount of resources is being allocated to the study of ice accretion in nautical and civil applications. As an example, ice accretion produces relevant effects on cables used in energy distribution nets and it affects the efficiency of wind turbines in alpine regions [7, 11].

A deeper knowledge of the icing phenomenon may enable the development of new anti-icing techniques and may guide the future design of innovative de-icing system, leading to more efficient solutions and a significant reduction of costs and environmental impact.

In order to study the ice accretion phenomenon and to develop ice protection on-board systems, different types of approach can be adopted: physical modeling, experiment or Computational Fluid Dynamics (CFD) simulations. The experimental approach includes in-flight tests, where a typical experiment consists of a flying tank that precedes the test aircraft. Ice is produced over the test aircraft by releasing water spray in favorable conditions. Experiments can be also conducted in refrigerated wind tunnels, where water droplets are released in the stream. This kind of experiments usually involve only portions of the entire geometry, such as wing sections or engine nacelles or antennas.

To complement experimental activities, numerical simulations are also carried out and are exstensively used in the design phase. Examples are the LEWICE [4,22,23], GlennICE [21], FENSAP-ICE [24] and MULTI-ICE [14,17] softwares. LEWICE is an ice prediction code developed at NASA since 1983. It is a 2D solver based on the standard Messinger model [13] and it can tackle simple three-dimensional geometries by means of a 2D-strip approach. The flow is solved by means of a potential solver; it is however possible to couple LEWICE with an external flow viscous solver. GlennICE is the LEWICE's successor and it has been developing at NASA Glenn Research Center since 1999. It is a full three-dimensional solver and it implements the standard Messinger model with slight modifications in the thermal fluxes. A strong limitation of GlennICE code is that it is capable of running only single time-step simulations because of its lack of a full-three dimensional routine for geometry reshaping. FENSAP-ICE is a three-dimensional ice accretion solver [2]. It was initially developed at McGill University and it implements a modified Messinger model. The complete Reynolds-Averaged Navier-Stokes (RANS) equation system is solved to compute the aerodynamic flow field. MULTI-ICE is a software developed by CIRA, the the Italian Aerospace Research Center, which contributes to the EXTICE (EXTreme ICing Environment) international project. MULTI-ICE uses a panel method for the computation of the aerodynamic field and is capable of evaluating the ice accretion on single or multi-element airfoils. This software implements the classical Messinger model and can also be coupled with a RANS solver for the evaluation of the aerodynamic field [14, 17].

At Politecnico di Milano, a novel framework for ice accretion simulations is currently under development, with the aim of providing a flexible interface among different CFD and ice-accretion models [5,9]. The PoliMIce (Politecnico di Milano Ice accretion software) library provides a built-in ice accretion engine which moves from the well-known Myers approach [15] and it includes state-of-the-art ice formation models. It solves the fully three-dimensional two-phase flow equations over the solid body, accounting for both rime and glaze ice formation.

In the present paper, the main features and the organization of the PoliMIce software are presented. Modifications to the original Myers's model include the assumption of a parabolic temperature profile to guarantee the consistency with respect to the wall boundary conditions. Moreover, the mass balance is generalized to conserve the liquid fraction at the interface between the glaze and the rime ice types. Numerical simulations are presented using the CFD open-source software OpenFOAM regarding in-flight ice accretion over two-dimensional airfoils and three-dimensional straight- and swept-wings.

The first section reports the general structure of the PoliMIce framework. Section 3 provides a brief review of the existing ice accretion models and shortly describes the PoliMIce implementation. Section 4 presents two- and three-dimensional simulations of in-flight icing. Numerical results are compared to simulations results from other software and to available experimental data.

2 Icing simulation framework

Ice accretion is a time dependent problem: as ice starts to form, the shape of the surface changes and therefore the aerodynamic flow field around the body is altered. Since droplet trajectories strongly depend on the local value of the flow velocity, each trajectory is modified and the impact point is displaced, thus eventually altering the ice accretion rate. Therefore, two different time scales can be singled out: the aerodynamic and the ice formation ones. The former is the time scale during which variations in the aerodynamic performances due to shape modifications are attained, the latter is the characteristic time resulting in significant ice accretion over the surface. The ice accretion problem is therefore usually solved using an iterative process: first, the aerodynamic flow field is computed over the initial or "clean" surface.

The distribution of water over the surface can be reconstructed by computing the trajectories of droplets and their impingement points. The information about water distribution is represented by the so-called collection efficiency β, which has the dimensions of a surface density. From the aerodynamic solution, the heat transfer coefficient, the recovery factor and the wall shear stress are also computed. The wall shear stress drives the dynamics of the liquid film layer. Under the thin film approximation it represents indeed the sole external force over the free water surface and it dominates its behavior.

From the above data, the ice accretion step is performed and the process is re-started over the new geometry.

[Fig. 1 about here.]

In figure 1 the flowchart explaining the structure of the PoliMIce software is shown. All data regarding the environmental conditions (the temperature, the pressure and the airspeed), the droplets characteristics and the simulation parameters, are passed to the CFD engine together with the meshed geometry (block *DATA* in figure 1)

The collection efficiency, the heat transfer coefficient, the recovery factor and the shear stress at the wall can be determined by means of a RANS simulation of the aerodynamic flow field (block *OpenFOAM* in figure 1). In the present calculation, we used the open source CFD solver OpenFOAM [1].

The droplet trajectory is computed using a Lagrangian particle tracking solver, according to the formulation presented in [10] (block *OpenFOAM: Particle tracking* in figure 1). To compute the collection efficiency, the flow field ahead of the solid surface is inseminated uniformly with a large number of droplets (ranging from thousands for 2D cases to three-four millions for 3D ones). Finally, by counting the number of droplets collected by a certain surface cell, it is possible to compute the total amount of mass that is collected by each computational cell in the unit time, namely, the collection efficiency β. By repeating this procedure for all the cells representing the solid surface, it is possible to reconstruct the distribution of water over the surface at each time step.

The output of the CFD simulations is then post-processed by the CFD/PoliMIce interface which recovers the superficial mesh from the three-dimensional one (block *Interface: surface mesh* in figure 1) and computes the extrapolated values of the collection efficiency in every cell belonging to the solid body (block *Interface: Accretion parameters* in figure 1). The values of the heat transfer coefficient and of the recovery factor are assumed to be constant over the entire domain and equal to 1000 $[W/m^2K]$ and 0.8, respectively. CFD simulations showed that these quantities are indeed uniform in the flow-field, with the only exception of very small regions close to the leading edge and in the laminar regime, which is relevant for the clean surface only.

At each time step, from the above aerodynamic data, PoliMIce computes the new ice thickness and the amount of liquid water in each cell (block *PoliMIce: Ice accretion computation* in figure 1). The ice accretion model implemented in PoliMIce is described in the next section and it is based on the well-known model of Myers [15]. The new shaped surface is then computed by moving the grid nodes along a fixed direction, which is the normal direction with respect to the "clean" configuration. Then a geometry smoothing algorithm is invoked in order to regularize the grid and remove non-physical region, such as interpenetration or cuts, that may possibly arise during the mesh displacement (block *PoliMIce: Geometry updating* in figure 1).

The new surface is finally processed by a mesh morphing algorithm which modifies the domain mesh (block *Mesh morphing* in figure 1). The latter is eventually passed over to the CFD solver to be used in the next iteration.

The PoliMIce is a fully three-dimensional solver, characterized by highly modular framework: indeed calculation regarding a full three-dimensional airplane, entailing the use of CFD++ as CFD solver have been already done in [3].

The framework is written in C++ object oriented language and it defines a general interface for coupling ice-accretion, grid alteration and CFD computations. The framework is modular and the input/output structure can be easily customized by the user. In particular, all the input data can be modified by means of text dictionaries without the necessity of re-compiling. A bash script is used to loosely couple the different modules of the framework.

3 Ice accretion models

The first mathematical formulation of the liquid water-ice two-phase problem was given by J. Stefan in 1889, on the basis of the fundamental formulations proposed by F. Neumann, B.P. Clapeyron and G. Lamé, among others. Starting from the results of Stefan's work regarding ice formation in the polar sea, the so-called Stefan's problem was generalized to describe physical systems where phase change can possibly occur, such as e.g. chemical processes, solid/liquid metal interfaces. Messinger in 1953 proposed a formulation of the Stefan's problem for aeronautical applications [13]. In 2001, Myers presented modified the Messinger's model to obtain a more accurate transition from the rime to the glaze regime and to improve the prediction of the heat transfer at the aircraft surface [15]. A new ice accretion model is derived in the present work which accounts for the two different mechanisms associated to rime and glaze ice formation and a new temperature profile within the ice sheet is proposed.

[Fig. 2 about here.]

Following [15], the complete superficial domain is first divided into elementary cells. For simplicity, in the present work the computational cells are coincident with the elements of the CFD mesh of the surface. Over each cell, a piece-wise constant representation of the solution is assumed. Then, a one-dimensional ice accretion problem is solved over each cell in the direction normal to the surface, see figure 2. Starting from a partitioning of the surface which results in polygons and projecting inward into the domain along the normal direction, the elementary sub-domain cells are obtained and the accretion model is resolved for each of these cells.

In the next sections, the Stefan's problem is briefly recalled to introduce the Messinger's and the Myers's models in section 3.1. In section 3.2, the new model is presented.

[Table 1 about here.]

3.1 Myers's model

The Stefan problem is defined by a set of four partial differential equations which describe the evolution of a single-component two-phase system as follows

$$\begin{cases} \dot{m}_{fr} + \dot{m}_h = \dot{m}_{in} - \dot{m}_{out} \\ \dfrac{\partial \theta}{\partial t} = \dfrac{K_w}{\rho_w C_{P_w}} \dfrac{\partial^2 \theta}{\partial z^2} \\ \dfrac{\partial T}{\partial t} = \dfrac{K_i}{\rho_i C_{P_i}} \dfrac{\partial^2 T}{\partial z^2} \\ \dot{Q}_{change} = \dot{Q}_{up} + \dot{Q}_{down} \end{cases} \tag{1}$$

where all relevant quantities are defined in the nomenclature. Typical values for the parameters are reported in Table 1.

The first equation in (1) is the continuity equation which enforces mass conservation. The second and the third equations model the one-dimensional heat diffusion in the liquid and solid phase, respectively, in the direction z normal to the surface. The last equation is the so-called Stefan condition. The Stefan conditions enforces the heat conservation law across the interface, Under the assumption that the phase change occurs over an interface of infinitesimal thickness. Indeed, the condition guarantees that the latent heat due to the phase change $\dot{Q}_{change}$ is equal to the net flux of heat from and towards the upper ($\dot{Q}_{up}$) and lower ($\dot{Q}_{down}$) layers.

The Messinger's model, proposed in 1953 [13], is based on a local energy balance, namely, it solves only the Stefano condition (last equation in (1)) namely,

$$\dot{Q}_l = \dot{Q}_c + \dot{Q}_e + \dot{Q}_d - \dot{Q}_k - \dot{Q}_a, \tag{2}$$

where $\dot{Q}_e$ is either the heat of evaporation (glaze ice regime) or the heat of sublimation (rime ice). The reader is referred to the Nomenclature section for the description of the diverse terms in (2) and to Reference [15] for their mathematical expressions. Diverse hypotheses are introduced to simplify the phase-change problem. The most relevant one is that the water and the ice have constant temperature in time and space. As a consequence, a discontinuous transition from rime to glaze ice is predicted. Moreover constant-temperature assumption prevents the heat to be conducted away from the phase changing interface and therefore the heat flux $\dot{Q}_{down}$. The heat flux $\dot{Q}_{up}$ includes among other terms the kinetic energy released by the impact of the droplets and the droplet latent heat. The model lacks however the sink term related to heat conduction from the interface to the wall surface across the ice sheet. The heat hence accumulates at the phase changing interface. As a consequence, the resulting ice accretion rate is underestimated, as observed by Myers [15].

The Myers's model [15] moves from the Stefan problem (1), which is simplified according to the following assumptions: the properties of ice and water do not depend on the temperature; the substrate (i.e. the wall) is at constant temperature, which for aeronautic applications it is usually assumed to be equal to the air temperature; droplets are in thermal equilibrium with the surrounding air and therefore their temperature is equal to the air temperature; the phase change occurs at a specified temperature, the water melting temperature; the temperature profile in both the ice and water layers can be approximated as a linear function of the distance from the substrate. Indeed, in aerospace applications, the water layer is usually assumed to be isothermal due to the very small thickness of the liquid film. Under the above hypotheses, the Stefan problem simplifies to

$$\begin{cases} \dfrac{\partial T}{\partial t} = \dfrac{K_i}{\rho_i C_{P_i}} \dfrac{\partial^2 T}{\partial {z_1}^2} \\ \dfrac{\partial \theta}{\partial t} = \dfrac{K_w}{\rho_w C_{P_w}} \dfrac{\partial^2 \theta}{\partial {z_2}^2} \\ L_F \rho_i \dfrac{\partial B}{\partial t} = K_i \dfrac{\partial T}{\partial z_1} - K_w \dfrac{\partial \theta}{\partial z_2} + \dfrac{\dot{Q}_{out} - \dot{Q}_{in}}{A} \\ \rho_i \dfrac{\partial B}{\partial t} + \rho_w \dfrac{\partial h}{\partial t} = \beta \text{ LWC } V_\infty \end{cases} \tag{3}$$

The reader is referred to the Nomenclature section for the description of the diverse terms in (2) and to Reference [15] for their mathematical expressions.

Myers introduced the so-called *rime limit thickness* B_g as a criterion for the selection of the proper accretion law, thus allowing for a smooth transition between the rime and the glaze regimes. In contrast, this transition occurs in a discontinuous way in the Messinger's model. The parameter B_g is defined as the maximum ice thickness that satisfies the Stefan problem if no liquid is present.

By observing that from the Fourier's law the heat flux is the thermal conductivity times the temperature gradient, it follows that the temperature profile—or, at least, its derivative at the phase changing interface—must be known. According to [15], under the assumption of a steady temperature profile, the heat equation in the ice layer can be approximated to the homogeneous leading order problem

$$\frac{\partial^2 T}{\partial z^2} = 0 \tag{4}$$

In the glaze regime, this leads to the following linear temperature profile within the ice layer

$$T(z) = \frac{T_{freezing} - T_{wall}}{B} z + T_{wall}$$

and hence

$$\dot{Q}_{down} = K_i \frac{\partial T}{\partial z} = K_i \frac{T_{freezing} - T_{wall}}{B}$$

Therefore, in the rime regime one has

$$\text{Rime:} \qquad \frac{\partial B}{\partial t} = \frac{\beta \text{ LWC } V_\infty}{\rho_{ri}} \tag{5}$$

whereas in the glaze regime the accretion law reads

$$\text{Glaze:} \qquad \frac{\partial B}{\partial t} = \frac{1}{\rho_{gi} L_F} \left(\dot{Q}_{down} + \dot{Q}_{up} \right) \tag{6}$$

where the limiting thickness is defined as

$$B_g = \frac{A K_i \left(T_{Freezing} - T_{wall} \right)}{A L_F \beta \text{ LWC } V_\infty - \dot{Q}_{up}} \tag{7}$$

which is computed by imposing $h = 0$ in (3), as detailed in [15]. In the model, if the limit thickness is negative or infinite, glaze ice can never appear; if B is smaller than B_g then rime ice is formed; if B is larger than B_g then glaze ice is formed.

3.2 An improved Myers model

A new model is now derived from the Stefan problem by following a procedure similar to the one proposed by Myers. The new model explicitly accounts for the mass fluxes related to sublimation, which is neglected in Myers's model.

Moreover, a more detailed description of the liquid film flow above the ice surface is introduced. In particular, differently from Myers's model, which accounts only for the water flowing from a glaze cell to an adjacent glaze cell, mass transfer from a rime to a glaze cell is allowed. Therefore, the new model guarantees mass conservation also in this case. To model the mass transfer, an additional term is included in the equation (5) for rime ice accretion. In rime cells, no outward mass flux is considered since in rime conditions the total amount of incoming liquid water freezes upon impact.

Finally, the third modification concerns the description of the heat diffusion problem through the ice phase in the glaze regime. In the Myers's model, the temperature of the wall remains constant during time. Therefore, for consistency, the solid wall must be characterized by a very high value of the thermal conductivity and by a very large thermal mass, so that the heat at the wall is rapidly conducted away into the solid continuum. In mathematical terms this means that the heat flux evaluated at the wall cannot have a finite value: from the Fourier's law, the derivative of the temperature profile cannot be finite at the solid boundary. In the description given by Myers, the temperature profile in the ice thickness a linear function of the distance from the wall, so its derivative assumes a finite, constant value. Unfortunately, a linear profile is not consistent with the hypothesis of a constant wall temperature discussed above.

Differently from Myers's approach, the heat diffusion equation in the ice layer (ref. 3) is discarded and, to circumvent the aforementioned inconsistency, the linear temperature profile is replaced by an assigned shape function. In this work, a parabolic temperature profile is introduced, namely, $T(z_1) = a\sqrt{z_1}+b$, where the constants a and b are computed from the following boundary values $T(0) = T_{Wall}$ and $T(B) = T_{Freezing}$ to obtain

$$T(z_1) = T_{Wall} + \frac{(T_{Freezing} - T_{Wall})}{\sqrt{B}}\sqrt{z_1} \tag{8}$$

The new model for the ice accretion in the rime regime therefore reads (cf. Myers model (5))

$$\text{Rime:} \qquad \frac{\partial B}{\partial t} = \left[\frac{\dot{m}_d + \dot{m}_{in} - \dot{m}_s}{A\rho_{ri}}\right]. \tag{9}$$

In the glaze regime one has (cf. relation (6))

$$\text{Glaze:} \qquad \frac{\partial B}{\partial t} = \frac{1}{\rho_g L_F}\left[k_i\frac{(T_{Freezing} - T_{Wall})}{2B} + \frac{\left(\dot{Q}_c + \dot{Q}_e + \dot{Q}_d - \dot{Q}_k - \dot{Q}_a\right)}{A}\right] \tag{10}$$

The limit thickness is computed as (cf. definition (7))

$$B_g = \frac{AK_i\left(T_{Freezing} - T_{wall}\right)}{2\left[L_F\left(\beta\ \mathrm{LWC}\ V_\infty A - \dot{Q}_s L_s^{-1}\right) - \left(\dot{Q}_c + \dot{Q}_s + \dot{Q}_d - \dot{Q}_k - \dot{Q}_a\right)\right]} \tag{11}$$

With respect to the original Myers model (5), (6), (7), it can be noted that additional terms are introduced that describe the sublimation and the evaporation. Moreover, in the accretion law for rime ice, a term is present accounting for the water that can possibly flow from a neighboring glaze cell. Finally, a scaling factor of $\frac{1}{2}$ is applied to the heat flux through the ice in the glaze regime (first term of equation (10)) and to the limiting thickness B_g. Both corrections result from the modification of the temperature profile from a linear to a parabolic profile. In (11), the term $\dot{m}_{in}$, which should be included in the denominator, is neglected because it resulted in excessive reduction of the limiting thickness B_g. Further investigations are required to assess its influence on glaze ice predictions.

Since the first term in (10) is always positive, the predicted accretion rate is lower than the one predicted by Myers model. Moreover, the limiting thickness

B_g is half the value obtained by the Myers' model, if the corrections due to the incoming mass flow and from sublimation are not taken into account. Therefore, glaze ice occurs at an earlier time with respect to the Myers model and, since the accretion rate for glaze ice is usually smaller than the rate for the rime ice, the overall ice accretion rate is expected to be smaller.

4 Numerical results

In the present section numerical results used for assessing the new ice accretion model and the PoliMIce framework are presented.

In two spatial dimensions, predictions from the improved and the standard Myers' modesl implemented in PoliMIce are compared to experimental results and to numerical results from NASA LEWICE code. Two-dimensional simulations of the symmetric NACA 0012 airfoil are reported in sections 4.1 and 4.2 for rime and glaze conditions, respectively. In section 4.3 , the GLC-305 airfoil is studied for a large ice accretion time. Three-dimensional results for a straight and a swept wing (ONERA M6) are presented in sections 4.4 and 4.5, respectively.

[Table 2 about here.]

[Fig. 3 about here.]

4.1 NACA 0012 in low temperature conditions

A symmetric NACA 0012 airfoil test case is studied first to assess the PoliMIce capabilities in rime ice conditions. The test conditions are gathered in table 2 and they are representative of winter conditions at low altitude, which can be encountered by small aircraft or airliners in take-off or landing.

In figure 3 a comparison of PoliMIce and LEWICE simulations with the experimental results is shown. The improved and the standard Myers' models implemented in PoliMIce deliver the same final ice shape because the two models are coincident in rime ice conditions. Close to the stagnation point, the predicted thickness compares fairly well to the experimental observation documented in [19],which is slightly overestimated. The LEWICE code predicts instead a lower thickness.

Away from the stagnation point, a so-called ridge type ice shape is observed in the experiments, according to the classification in [6]. Ridge-type ice shape are caused by liquid film instabilities that are not modeled in the PoliMIce software. In this particular region the outer flow is very complicated because of the occurrence of the peculiar double-horn ice shapes and flow separation. This makes the heat transfer coefficient and the recovery factor very hard to determine. Also, this non-regular region seems to be highly affected by the details of the droplet splash process. Differently from the stagnation point region—where the droplet impacts the surface along a normal trajectory and the rebounding droplets deposit near the impact point—droplets impact with an angle and the water spreads on a wider region downstream, since rebounding droplets are carried away by the outer air flow, see [16]. In these conditions, the correct collection efficiency is very difficult to estimate. On the contrary, the LEWICE software is capable of predicting the formation of the double-horn shape.

[Fig. 4 about here.]

[Table 3 about here.]

4.2 NACA 0012 in mild temperature conditions

The second test case regards the NACA 0012 operating at an angle of attack of 4 degrees in glaze conditions. Therefore, the observed ice shape is not symmetrical. All parameters are reported in table 3 for completeness.

In figure 4, results from PoliMIce and LEWICE are compared to the experimental results from [20]. Note that at the stagnation-point region the improved model accurately captures the ice thickness, which is instead over-predicted by the standard Myers' model. The improvement is possibly related to the 1/2 factor in the expression of the glaze ice accretion rate, as discussed in 3.2. Moreover, the Myers' model predicts a very smooth final ice shape, indicating excessive glaze ice accretion, possibly because of the same over-estimation of both the glaze ice accretion and of the rime ice limit B_g. The LEWICE code predicts similar value of the ice thickness at the stagnation point but instead it over-estimates the size of the ice horn in the upper boundary.

[Table 4 about here.]

[Fig. 5 about here.]

4.3 GLC-305

The third case reproduces an experimental test over a long period of time. The overall simulated time is 22 minutes and 30 seconds. Experimental data are presented in [12]. This kind of tests are of interest to understand the consequences of a possible failure of the ice protection system. The conditions for this simulation are listed in table 4 and are typical of rime ice formation.

In fig 5 the final ice shape predicted by the improved Myers' model is shown together with the experimental data obtained at the NASA IRT wind tunnel facility. The predicted ice shape compares fairly well to the experimental results presented in [12].

4.4 Straight wing

A three-dimensional case is now presented. The simulation involves a three-dimensional straight, constant chord wing in the conditions listed in table 5. The wing section is a NACA 0012 airfoil. The root section is studied, where the wing intersects the symmetry plane. This is a very simple geometry which is reported here as a reference for the swept wing case in the next section, where the influence of three-dimensional effects on the icing phenomenon, with particular reference to the region close to the symmetry plane of the wing, is studied.

[Table 5 about here.]

[Fig. 6 about here.]

[Fig. 7 about here.]

Figure 6 shows the predicted ice shape for the considered geometry. Since this case involves a straight wing which is perpendicular to the free-stream, three-dimensional effects are expected to be not relevant. Indeed results show a span-constant ice shape.

Figure 7 shows the predicted ice shape superimposed to the collection efficiency β. It is remarkable that ice is formed in a portion of the wing where droplets are not impinging, i.e., $\beta = 0$. Indeed, in glaze icing conditions, liquid water flows downstream over the surface, driven by the action of the external air stream, and a secondary single ridge is formed behind the main ice structure on the leading edge. This latter primary structure is also characterized by a saw-like shape because of the mixed rime/glaze nature of the icing process.

4.5 *Swept wing: Onera M6*

A fully three-dimensional case over the Onera M6 wing geometry is here presented. This wing is characterized by a swept angle of 26.7 degrees which produces relevant three-dimensional effects. In this configuration, the flow velocity is known to have relevant components in the direction of the wing span. The case is studied to highlight three-dimensional effects on the ice shape that is formed on the wing. Flight condition for this test case are listed in table 6 and are representative of a glaze ice accretion.

[Table 6 about here.]

[Fig. 8 about here.]

[Fig. 9 about here.]

The predicted ice shape is shown in figure 8. Three-dimensional effects are evident in the region very close to the symmetry plane, where the ice shape changes thickness abruptly. Starting from the symmetry plane, moving towards the wing tip, the ice shape is convex and then a discontinuity is observed in the iced portion of the leading edge. There, the ice layer is narrower and the ice surface is concave. Proceeding along the leading edge, the ice layer is again convex and then turns concave for the entire wing span. This particular behavior is thought to be related to the flow of liquid water over the ice surface. The liquid film is dragged along the flow and away from the symmetry plane towards the tip of the wing. Figure 9 shows the component of wall shear stress along the z-axis (which correspond to the wing axis too), to support the above explanation.

5 Final remarks

The suite PoliMIce, a software environment for simulating fully three-dimensional ice accretion problems, was presented. The PoliMIce environment is intended as a versatile research and design tool, which can be used as a framework for the further development of ice accretion models. According to this idea, the highly modular structure of PoliMIce was designed to easily include different CFD solvers and ice accretion models. The former include the CFD software OpenFOAM, CFD++ [3]) and two-dimensional potential-flow solvers. Moreover, a novel ice accretion model was derived and implemented in PoliMIce, starting from Myers's ice accretion model.

The new model includes a consistent definition of the temperature profile and guarantees mass conservation across rime/glaze cells. In the considered cases, the model is demonstrated to provide more accurate results over the Myers' model, at least in the region close to the stagnation point, where the phenomenon is characterized by simpler dynamics. Results obtained are in good agreement with the experimental results.

In the future, a multiple-zone model will be introduced to deal explicitly with the stagnation region, the so-called rough zone immediately downstream and the run-back ice region, where the anti-icing system is usually not installed in standard aeronautical configurations. Improvement to the physical model will include liquid film instabilities and rivulet formation, the modeling of the anti-icing system and a reduced order model (ROM) of the splashing of SLD (Supercooled Large Droplets).

6 Acknowledgments

The authors would like to thank Gianluca Parma for implementing the new input procedure for defining the case data.

References

[1] The openfoam foundation. `http://www.openfoam.org/`.

[2] C. N. Aliaga, M. S. Aubé, G. S. Baruzzi, and W. G. Habashi. FENSAP-ICE-Unsteady: Unified In-Flight Icing Simulation Methodology for Aircraft, Rotorcraft, and Jet Engines. *Journal of Aircraft*, 48(1):119–126, 2011.

[3] M. Bernasconi. Sviluppo di un ambiente di simulazione per l'accrescimento di ghiaccio su velivoli completi. Master's thesis, Politecnico di Milano, 2013.

[4] C. S. Bidwell and M. G. Potapczuk. User Manual for the NASA Lewis Three-Dimensional Ice Accretion Code (LEWICE 3D). Technical report, NASA, 2008.

[5] E. Borghi, A. Guardone, and G. Quaranta. Assessment of an improved Myers model for airfoil icing. *3rd CEAS Air and Space Conference*, 2011.

[6] M. B. Bragg, A. P. Broeren, and L. A. Blumenthal. Iced-airfoil aerodynamics. *Progress in Aerospace Sciences*, 41:323–362, 2005.

[7] G. Fortin C. Hochart and J. Perron. Wind Turbine Performance under Icing Conditions. *Wind Energy*, 2007.

[8] T. Cebeci and F. Kafyeke. Aircraft Icing. *Annu. Rev. Fluid Mech.*, 2003, 35:11-21.

[9] M. Garabelli and G. Gori. PoliMIce: un ambiente di simulazione per la previsione dell'accrescimento di ghiaccio su velivoli. Master's thesis, Politecnico di Milano, 2013.

[10] R.W. Gent, N.P Dart, and J.T. Cansdale. Aircraft icing. *Phil. Trans R Soc Lond A 358:2873 2911*, 2000.

[11] W.J. Jansinski, S.C. Noe, M.S. Selig, and M.B. Bragg. Wind turbine performance under icing conditions. *Journal of Solar Energy Engineering*, 1998.

[12] H. E. Addy Jr. Ice Accretions and Icing Effects for Modern Airfoils. Technical Publication NASA/TP-2000-210031, 2000.

[13] B.L. Messinger. Equilibrium Temperature of an Unheated Icing Surface as a Function of Air Speed. *Journal of the Aeronautical Sciences, pp 29-42*, January, 1953.

[14] G. Mingione and V. Brandi. Ice Accretion Prediction on Multielement Airfoils. *Journal of Aircraft*, 1998.

[15] T. G. Myers. Extension to the Messinger Model fort Aircraft Icing. *Cranfield University, England MK43 0AL, United Kingdom*, AIAA Journal, Vol. 39, No. 2, 2001.

[16] T. Okawa, T. Shiraishi, and T. Mori. Effect of impingement angle on the outcome of single water drop impact onto a plane water surface. *Exp Fluids, 44:331-339*, 2008.

[17] F. Petrosino, G. Mingione, A. Carozza, T. Gilardoni, and G. D'Agostini. Ice Accretion Model on Multi-Element Airfoil. *Journal of Aircraft*, 2011.

[18] K. Politovich. Predicting Glaze ore Rime Ice Growth on Airfoils. *Journal of Aircraft, Vol. 37, No. 1*, 2000, pp 117-121.

[19] G. A. Ruff and B. M. Berkowitz. Users Manual for the NASA Lewis Ice Accretion Prediction Code (LEWICE)]. *NASA Contractor Report 185129*, 1990.

[20] J. Shin and T. Bond. Experimental and computational ice shapes and resulting drag increase for a NACA0012 airfoil. Technical Publication NASA/TM-105743, 1992.

[21] M. G. Potapczuk W. B. Wright and L. H. Levinson. Comparison of LEWICE and GlennICE in the SLD Regime. Technical report, NASA, 2008.

[22] W. B. Wright. User Manual for the NASA Glenn Ice Accretion Code LEWICE, version 2.2.2. Technical report, NASA, 2002.

[23] W. B. Wright. User's Manual for LEWICE, version 3.2. Technical report, NASA, 2008.

[24] H. Beaugendre Y. Bourgault and W. G. Habashi. Verification and Validation of NASA LEWICE 2.2 Icing Software Code. *Journal of Aircraft*, 2000.

List of Figures

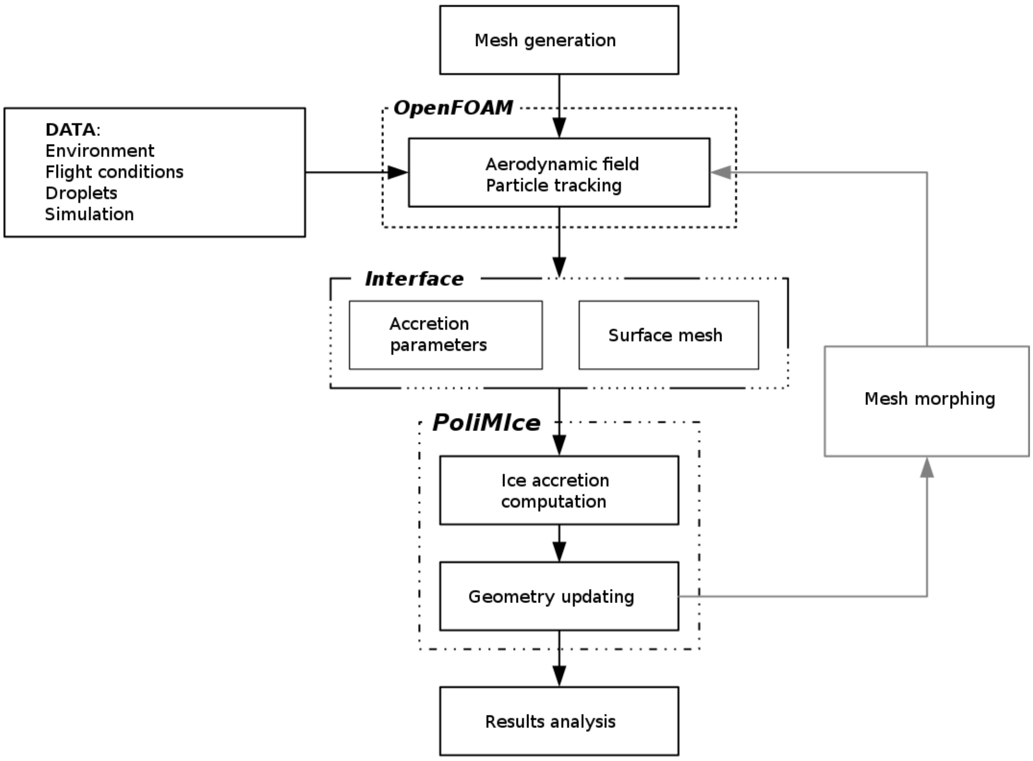

Fig. 1. Framework flowchart: this picture shows the logical steps through which the solution to the ice accretion problem is obtained

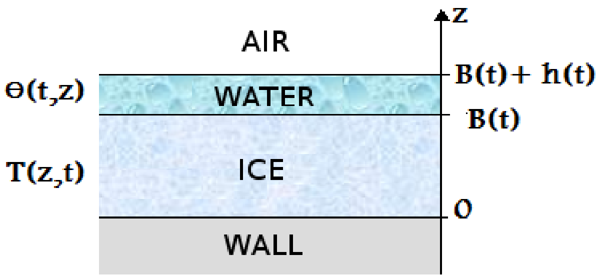

Fig. 2. Elementary cell for the discrete ice problem. The cell reference system is also depicted. Over each elementary cell composing the entire surface the Stefan problem (1) is solved.

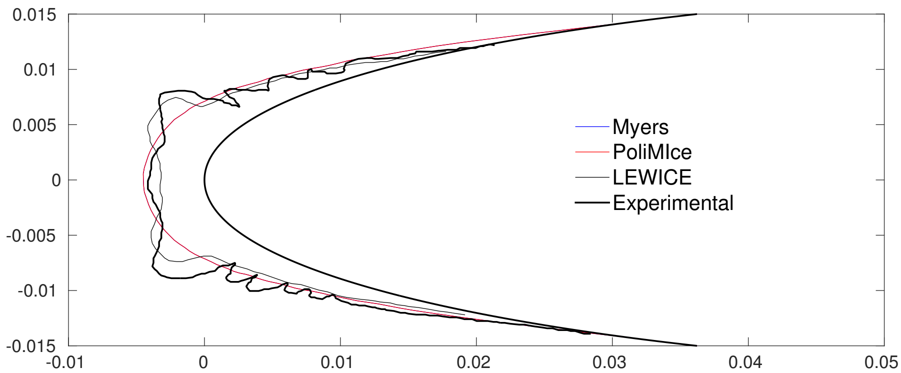

Fig. 3. Comparison of the experimental results for the rime ice case from [19] and numerical results from the Myers' model (blue line), the improved Myers model in (PoliMIce,red line) and LEWICE (black line). The experimental shape is shown as thick black line. In rime ice conditions, the improved and the standard Myers' models are the same.

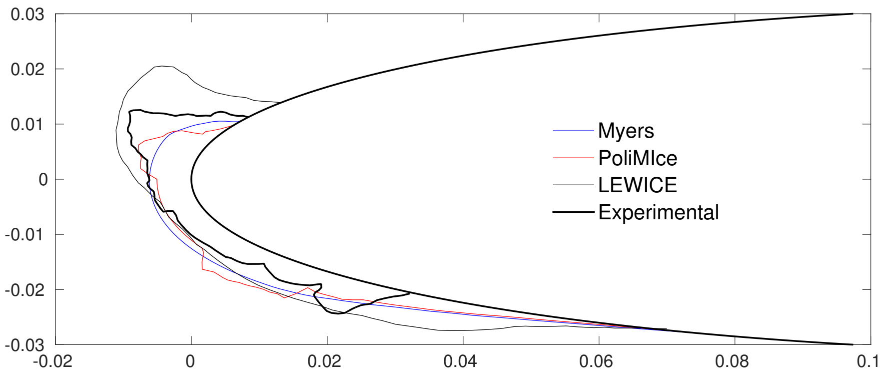

Fig. 4. Comparison of the experimental results for the mild temperature case from [20] and numerical results from the Myers' model (blue line), the improved Myers model in (PoliMIce,red line) and LEWICE (black line). The experimental shape is shown as thick black line.

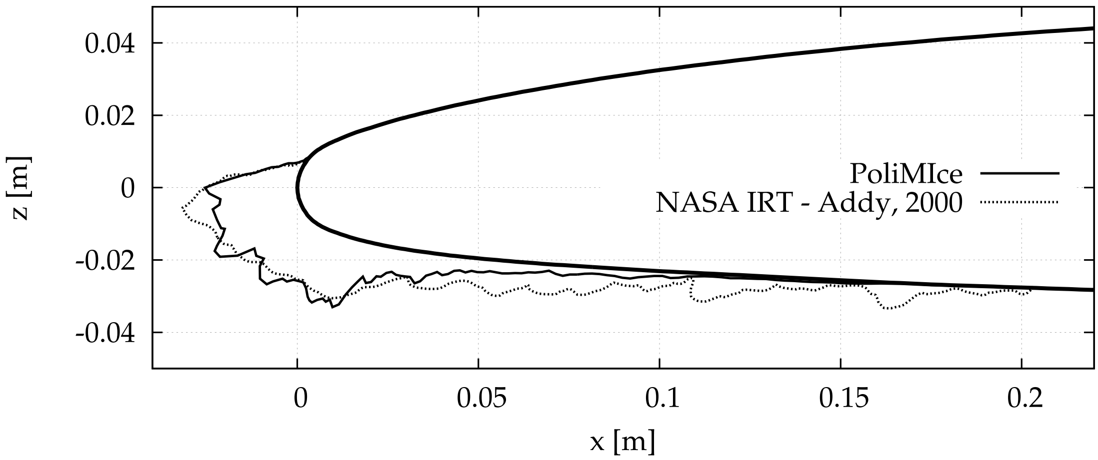

Fig. 5. Comparison with experiment: comparison of PoliMIce predicted ice shape and experimental results obtained at NASA IRT [12].

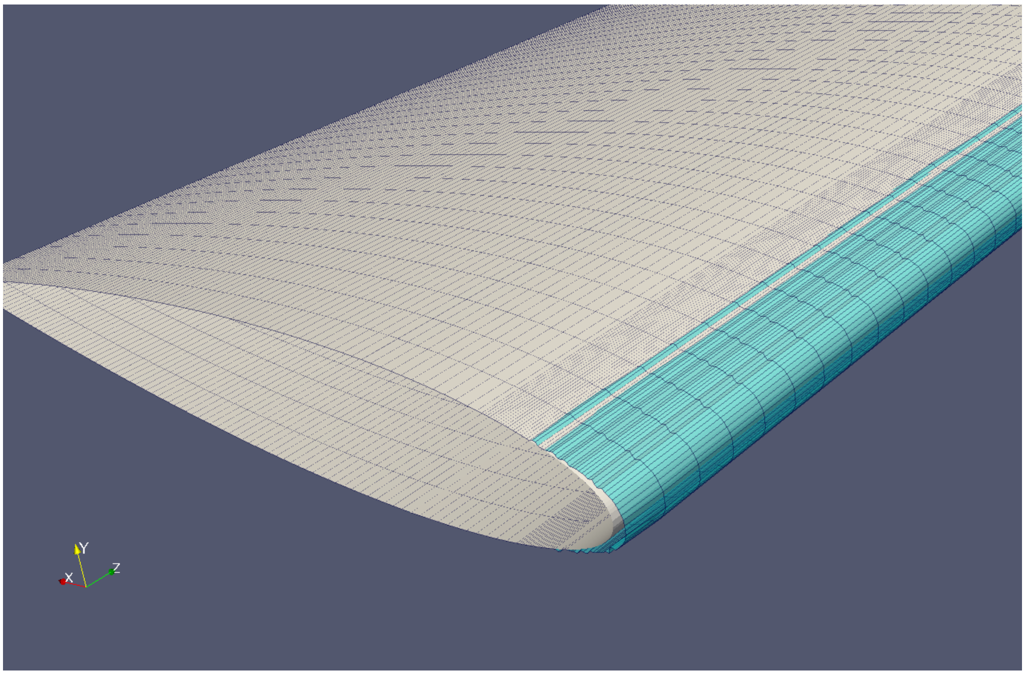

Fig. 6. Predicted ice shape for test case 4. This picture shows an enlargement of the region close to the center line of the wing.

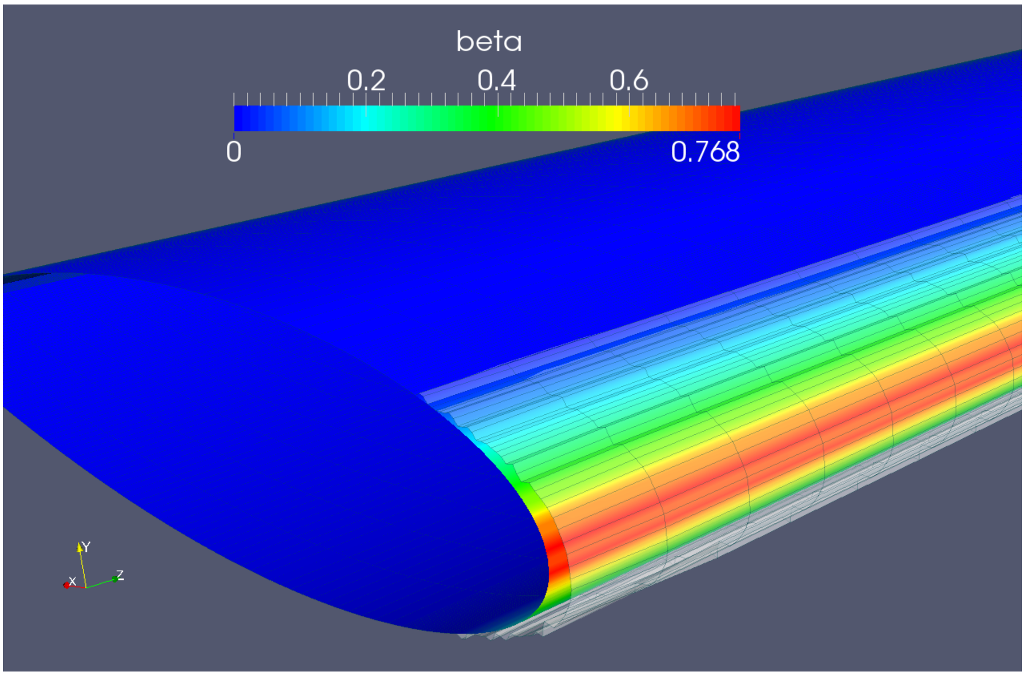

Fig. 7. Test case 4. This picture shows an enlargement of the region close to the center line of the wing and compare the collection efficiency with the resulting ice shape, highlighting the relation between ice thickness and β.

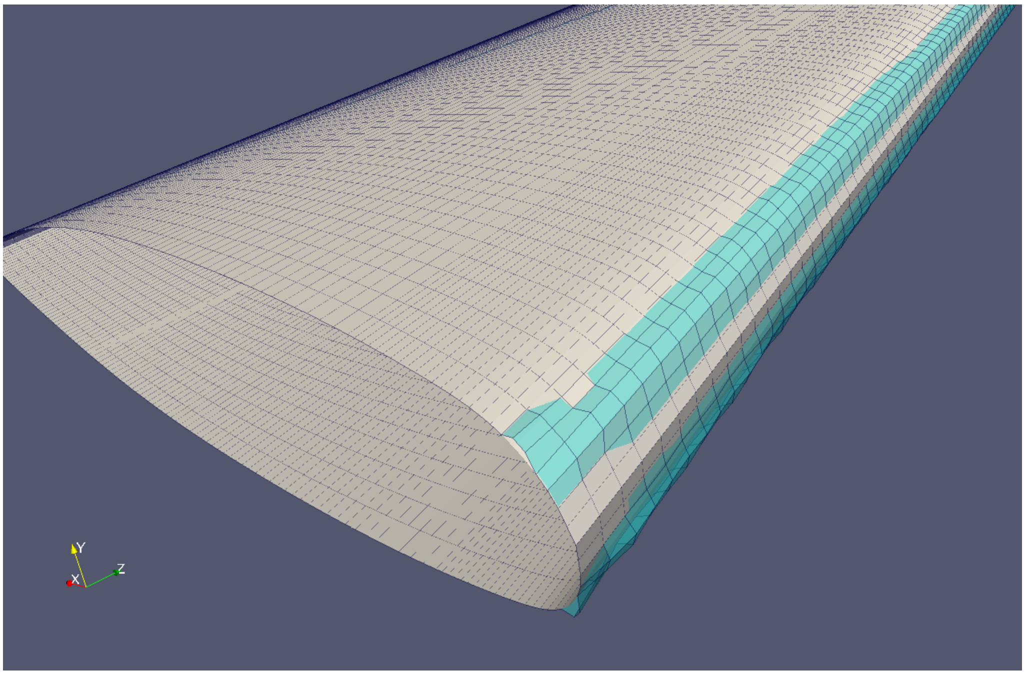

Fig. 8. Predicted ice shape for test case 5. This picture shows an enlargement of the region close to the symmetry plane of the wing.

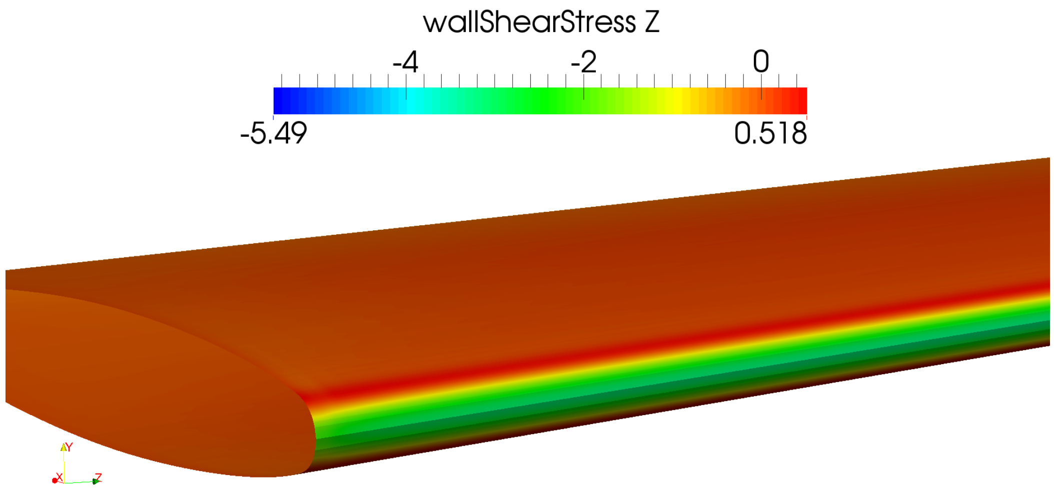

Fig. 9. z component of wall shear stress for Onera M6 at flight condition reported in table 6. The picture is an enlargement of the region close to the symmetry plane of the wing

List of Tables

Density	ρ_w	1000 $[Kg/m^3]$	$\rho_{i_{rime}}$	880 $[Kg/m^3]$
	$\rho_{i_{glaze}}$	917 $[Kg/m^3]$		
Latent heat	L_S	$2.83 \cdot 10^3$ $[J/Kg]$	L_F	$3.344 \cdot 10^5$ $[J/Kg]$
	L_E	$2.26 \cdot 10^6$ $[J/Kg]$		
Specific heat	C_{P_w}	4218 $[J/KgK]$	C_{P_i}	2050 $[J/KgK]$
Thermal conductivity	K_w	0.571 $[W/mK]$	K_i	2.18 $[W/mK]$

Table 1
In this table, values used for each parameters during simulation presented in this paper are listed.

α [deg]	V_∞ [m/s]	T_∞ [K]	P_∞ [Pa]	MVD [μm]	LWC [g/m^3]	time [s]
0	129	260.55	90700	20	0.5	120

Table 2
Flight condition for test case 1 [19]: values represent rime ice condition and are typical of low altitude flight.

α [deg]	V_∞ [m/s]	T_∞ [K]	P_∞ [Pa]	MVD [μm]	LWC [g/m^3]	time [s]
4	67	269.3	100000	20	1	360

Table 3
Flight condition for test case 2 [19]

α [deg]	V_∞ [m/s]	T_∞ [K]	P_∞ [Pa]	MVD [μm]	LWC [g/m^3]	time [s]
6	90	263.15	100000	20	0.43	1350

Table 4
Flight condition for test case 3 [12]: this is a case where ice begin to grow as rime ice and, once reached the rime ice limit thickness continues to grow as glaze ice.

α [deg]	V_∞ [m/s]	T_∞ [K]	P_∞ [Pa]	MVD [μm]	LWC [g/m^3]
0	120	260.55	100000	20	0.5

Table 5
Flight condition for test case 4: this is a case where ice begin to grow as rime ice and, once reached the rime ice limit thickness continues to grow as glaze ice.

α [deg]	V_∞ [m/s]	T_∞ [K]	P_∞ [Pa]	MVD [μm]	LWC [g/m^3]
0	50	260.55	100000	20	0.5

Table 6
Flight condition for test case 5: ice begin to grow as rime ice and, once reached the rime ice limit thickness continues to grow as glaze ice.